Sodium butyrate induces ferroptosis in endometrial cancer cells via the RBM3/SLC7A11 axis

Ziwei Wang
Wuhan Union Hospital
Wan Shu
Wuhan Union Hospital
Rong Zhao
Wuhan Union Hospital
Yan Liu
Wuhan Union Hospital
Hongbo Wang (hb_wang1969@sina.com)
Wuhan Union Hospital

Research Article

Keywords: Sodium Butyrate, Ferroptosis, Glutathione metabolism, RBM3, SLC7A11

Posted Date: March 15th, 2023

DOI: https://doi.org/10.21203/rs.3.rs-2681132/v1

Additional Declarations: No competing interests reported.

Version of Record: A version of this preprint was published at Apoptosis on May 11th, 2023. See the published version at https://doi.org/10.1007/s10495-023-01850-4.

Abstract

Ferroptosis is a form of programmed cell death with important biological functions in the progression of various diseases, and targeting ferroptosis is a new tumor treatment strategy. Studies have shown that sodium butyrate plays a tumor-suppressing role in the progression of various tumors, however, the mechanism of NaBu in endometrial cancer is unclear. Cell viability, clone formation, proliferation, migration, invasion abilities and cell cycle distribution were assessed by CCK8 assay, Clone formation ability assay, EdU incorporation, Transwell chambers and flow cytometry. The level of ferroptosis was assayed by the levels of ROS and lipid peroxidation, the ratio of GSH/GSSG and the morphology of mitochondria. Molecular mechanisms were explored by metabolome, transcriptome, RNA-pulldown and mass spectrometry. The in-vivo mechanism was validated using subcutaneous xenograft model. In this study, NaBu was identified to inhibit the progression of endometrial cancer in vitro and in vivo. Mechanistically, RBM3 has a binding relationship with SLC7A11 mRNA. NaBu indirectly downregulates the expression of SLC7A11 by promoting the expression of RBM3, thereby promoting ferroptosis in endometrial cancer cells. In conclusion, Sodium butyrate can promote the expression of RBM3 and indirectly downregulate the expression of SLC7A11 to stimulate ferroptosis, which may be a promising cancer treatment strategy.

Highlights

- Sodium butyrate promotes endometrial cancer cell ferroptosis.
- RBM3 has a binding relationship with SLC7A11 mRNA and negatively regulates SLC7A11 expression.
- Sodium butyrate promotes endometrial cancer cell ferroptosis via the RBM3/SLC7A11 axis.

1. Introduction

Endometrial cancer is one of the most common malignant tumors of the female reproductive tract[1]. It seriously endangers women's health and presents great challenges in public health[2]. Endometrial cancer mainly occurs in perimenopausal and postmenopausal women, and the early symptoms are relatively insidious, mostly manifesting as irregular vaginal bleeding and vaginal discharge[3, 4]. Endometrial cancer is mainly treated with surgery. Generally, the prognosis is good; however, there are still some patients who are diagnosed at an advanced stage and have poor prognosis[5, 6]. Therefore, it is very important to explore the molecular mechanism of the occurrence and development of endometrial cancer.

Recently, the gut microbiota has become one of the hotspots in this research area. It plays an important role in a variety of diseases. In colorectal cancer, *L. gallinarum* in the gut can promote apoptosis of colorectal tumor cells by producing the protective metabolite indole-3-lactic acid (ILA)[7]. Short-chain fatty acids produced by the gut microbiota activate the MAPK-PI3K signaling pathway by promoting the production of IGF1 to stimulate the progression of prostate cancer[8]. A previous study by our group found that the abundance of butyric acid-producing bacteria was significantly reduced in a mouse model

of endometrial dysplasia induced by a high-sugar and high-fat diet(unpublished manuscript). Endometrial dysplasia is an endometrial cancer precancerous lesion[9]. Butyric acid is an important histone deacetylase inhibitor that exerts a tumor suppressor role in a variety of tumors[10–12]. Therefore, we speculate that butyric acid may play a tumor suppressor role in the progression of endometrial cancer.

Ferroptosis, a new form of programmed cell death, has attracted widespread attention and is characterized by iron-dependent lipid peroxidation reaching lethal levels[13]. SLC7A11 encodes a chloride-dependent cystine/glutamate transporter, which promotes the intracellular transport of cystine and converts it into cysteine, which then enzymatically reacts with glutamate and glycine to generate glutathione[14]. SLC7A11-mediated glutathione biosynthesis is closely related to ferroptosis[15, 16]. With the deepening of research, scientists have found that ferroptosis plays an important role in the occurrence and development of various diseases[17]. In hepatocellular carcinoma, ETS1 inhibits ferroptosis through the ETS1/miR-23a-3p/ACSL4 axis and mediates the resistance of hepatoma cells to sorafenib[18]. Ferroptosis also plays an important role in the occurrence and development of endometrial cancer[19]. However, the role of ferroptosis in endometrial cancer is largely unknown.

RNA-binding proteins are a class of proteins that are widely involved in the occurrence and development of various diseases through the regulation of RNA post-transcriptional modifications[20–22]. In the appearance and development of malignant tumors, the role of RNA-binding proteins cannot be underestimated. In ovarian cancer, CELF2 increases the stability of FAM198B mRNA by binding to the 3'UTR of FAM198B mRNA and inhibits tumor progression[23]. RBM3 is an important RNA-binding protein that has dual roles in tumors[24–27]. However, no studies have explored the role of RBM3 in endometrial cancer.

In this study, we found that in endometrial cancer cells, NaBu inhibits the progression of endometrial cancer by promoting ferroptosis, explored the molecular mechanism of NaBu, and revealed that NaBu promotes ferroptosis via the RBM3/SLC7A11 axis.

2. Materials And Methods

2.1. Cell Culture and Chemical Reagents

Ishikawa and HEC-1B cells were purchased from Zhong Qiao Xin Zhou Biotechnology, and both were identified by short tandem repeat analysis. All cells were cultured in a 37°C incubator with 5% CO2. Ishikawa and HEC-1B cells were cultured in DMEM/F12 (BasalMedium) and MEM (BasalMedium) containing 10% FBS (BIOIND). Only cells under 10 passages were used for the experiments. NaBu (MACKLIN, S817488) was dissolved in ultrapure water and used at a concentration of 5 mM. Deferoxamine mesylate (DFO, Selleck, Ba33112) was dissolved in Dimethyl sulfoxide (DMSO) and used at a concentration of 200 μM.

2.2. Cell viability and Clone formation ability assays

Cell viability was detected using a Cell Counting Kit-8 assay (CCK8, Selleck, B34302). Cells were seeded in a 96-well culture plate (3000 cells/well), and CCK-8 reagent was added according to the manufacturer's instructions. The absorbance at 450 nm was measured using a microplate reader. Cells were seeded in 6-well plates (500 cells/well) and cultured for 14 days. The cells were rinsed with phosphate-buffered saline (PBS, Servicebio) and fixed with 4% paraformaldehyde (Servicebio) for 15 minutes. Then, the cells were stained with 0.1% crystal violet solution (Servicebio), rinsed with PBS and allowed to dry.

2.3. Cell Proliferation Assay

BeyoClick™ EdU Cell Proliferation Kits with Alexa Fluor 555 (Beyotime, C0075S) were used to detect cell proliferation. According to the manufacturer's instructions, an equal volume of 2X EdU working solution (20 μM) was added to the plate and incubated for 3 hours. Then, the cells were fixed, washed and stained with Hoechst 33342. Images were collected under a fluorescence microscope.

2.4. Migration and Invasion ability assays

Cell migration was detected using Transwell chambers (Corning, 3422). The cells were diluted in serum-free medium (30,000 cells/150 μL) and added to the upper chamber. Then, 700 μL of medium containing 20% FBS was added to the lower chamber. The cells were placed in the incubator for 24 hours. Then, the chamber was rinsed with PBS, fixed with 4% paraformaldehyde, stained with 0.1% crystal violet solution, rinsed with PBS and left to dry. Images were collected under a microscope. The cell invasion assay was conducted in the same manner as the migration assay, and with the addition of Matrigel (BD Biosciences) to the upper chamber.

2.5. Cell cycle assay

The cell cycle was detected using PI/RNase Staining Buffer Solution (BD Biosciences, 550825). The cells were seeded in six-well plates. The cells were digested, washed and fixed with PBS containing 70% alcohol for 24 hours at 4°C. Then, the cells were washed, centrifuged and incubated with PI/RNase Staining Buffer Solution for 15 minutes.

2.6. Metabolomics and Transcriptomics

Metabolomic sequencing and transcriptomic sequencing were performed by Shanghai Applied Protein Technology Co. Ltd.

2.7. Reverse Transcription and qRT-PCR

Total RNA of cell samples was extracted using TRIzol (Invitrogen) according to the manufacturer's instructions. cDNA was obtained using ABScript III RT Master Mix for qPCR (ABclonal, RK20428). qRT–PCR was performed using 2X Universal SYBR Green Fast qPCR Mix (ABclonal, RK21203) and a CFX Connect Real-Time PCR Detection System (BioRad). The mRNA expression levels relative to ACTH were calculated using the 2-ΔΔC t method. Primers used were as follows:

SLC7A11 forward 5'-GCGTGGGCATGTCTCTGAC-3' and reverse 5'-GCTGGTAATGGACCAAAGACTTC-3'; ACTH forward 5'- TGACGTGGACATCCGCAAAG-3' and reverse 5'- CTGGAAGGTGGACAGCGAGG-3'; and RBM3 forward 5'-TGAGAGCCATGAACGGAGAGT-3' and reverse 5'-GTAGCGGTCATAACCACCCTG-3'.

2.8. Western Blot

Cell samples were lysed using RIPA buffer (Servicebio), PMSF (Servicebio) and protease cocktail inhibitor (Selleck). Cells were collected by scraping. Supernatants were obtained after high-speed centrifugation, and protein concentrations were measured using a BCA Assay Kit (Thermo Fisher Scientific). Protein samples were fractionated using SDS–PAGE, transferred to polyvinylidene fluoride membranes (Millipore) and incubated at 4°C with anti-SLC7A11 (1:500, ABclonal), anti-RBM3 (1:400, ABclonal) and anti-GAPDH (1:20,000, ABclonal). The primary antibody was incubated overnight followed by incubation with horseradish peroxidase (HRP)-conjugated secondary antibodies (1:7500, ABclonal). Immunoreactive bands were detected using enhanced chemiluminescence detection reagents (Thermo Fisher Scientific). Image Lab software was used to analyze the results.

2.9. Glutathione Metabolism Assay

Glutathione metabolism was detected using GSH and GSSG Assay Kits (Beyotime, S0053). The cells were plated into a 6-well plate, digested and centrifuged. The supernatant was discarded. The protein removal reagent M solution was added to the cell pellet and vortexed immediately. The cell suspension was placed in liquid nitrogen and a 37°C water bath for two quick cycles. After freezing and thawing, the cell suspension was placed at 4°C for 5 minutes and centrifuged at 12000 × g for 10 minutes, and the supernatant was taken for the determination of the glutathione (GSH) and oxidized glutathione (GSSG) contents.

2.10. Transmission Electron Microscopy

The cells were plated and rinsed twice with precooled PBS, and 1 ml of electron microscope fixative (Servicebio, G1102-10ML) was added. The cells were scraped off in a clockwise direction, and the cell suspension was aspirated into a 1.5 ml centrifuge tube and centrifuged at 1500 rpm for 5 minutes. The supernatant was discarded, and 1 ml of fresh electron microscope fixative was added to the centrifuge tube followed by resuspension and fixation for 3 hours. The samples were sent to Servicebio for subsequent sample preparation and image acquisition.

2.11. Total reactive oxygen species assay

Total reactive oxygen species (ROS) were detected using a Reactive Oxygen Species Assay Kit (Beyotime, D3861). According to the manufacturer’s instructions, the DCFH-DA probe was diluted in serum-free medium at a ratio of 1:1000, incubated with the cells for 20 minutes at 37°C and mixed every 4 minutes. The cell suspension was centrifuged and washed twice with serum-free medium, and 300 μl of PBS was added to resuspend the cell pellet.

2.12. Lipid Peroxidation assay

The level of lipid peroxidation (lipid ROS) was measured using C11 BODIPY™ 581/591 (Thermo Fisher Scientific, S0033M). According to the manufacturer's instructions, C11 BODIPY581/591 was dissolved in DMSO to generate a stock solution at a concentration of 5 mM. The stock solution was diluted with serum-free medium at a ratio of 1:1000 and incubated with the cells for 30 minutes at 37°C. The cell suspension was centrifuged and washed twice with serum-free medium, and 300 μl of PBS was added to resuspend the cell pellet.

2.13. Intracellular Fe2 + assay

Intracellular Fe2 + was measured using Phen Green™ SK (Thermo Fisher Scientific, P14312). According to the manufacturer's instructions, Phen Green™ SK was dissolved in DMSO to generate a stock solution at a concentration of 5 mM, and the stock solution was diluted with serum-free medium at a ratio of 1:1000 and incubated with the cells for 30 minutes at 37°C. The cell suspension was centrifuged and washed twice with serum-free medium, and 300 μl of PBS was added to resuspend the cell pellet.

2.14. Plasmid transfection and viral transduction

The SLC7A11 overexpression plasmid and RBM3 silencing lentivirus were synthesized by Gene and cloned into CV061 and GV116 vectors, respectively. The RBM3 overexpression lentivirus was synthesized by GenePharma and cloned into the LV18 (CMV/Puro) vector. Plasmid transfection was performed using NEOFECT™ DNA transfection reagent (TF201201(TF20121201)). According to the manufacturer's instructions, polybrene was used for viral transduction.

2.15. RNA-Pulldown, silver staining and mass spectrometry

The cells were harvested, lysed, and centrifuged, and the cell supernatant was collected. Biotin-labeled RNA probes were incubated with magnetic streptavidin beads to form complexes. The biotin-labeled RNA probe-streptavidin magnetic bead complex was added to the cell supernatant to enrich the protein. The enriched protein was eluted and stored. Protein samples were fractionated using SDS–PAGE. SDS–PAGE was performed using a Fast Silver Stain Kit (Beyotime, P0017S). The steps were fixation, sensitization, staining, color development, and termination. Mass spectrometry was performed by SpecAlly.

SLC7A11: CGCGTAATACTTGAATCTCT-/3bio/; scramble: AGAGATTCAAGTATTACGCG-/3bio/

2.16. In vivo experiments

Female nude mice were purchased from GemPharmatech. The mice were randomly divided into groups, and a 1×10^7/150 μL cell suspension of Ishikawa cells was implanted into the right scapulas of the nude mice. One week later, NaBu was added to the drinking water at a concentration of 200 mM, and the drinking water was changed every two days. After 28 days of inoculation, the mice were sacrificed, and the tumor was removed, weighed and measured.

2.17. Statistic and Analysis

GraphPad Prism version 8 was used for statistical analysis. Statistical results were expressed using the mean ± standard error of the mean (mean ± SEM), and Student's t test was used to compare significant differences between two groups. $P < 0.05$ represents statistical significance.

3. Results

3.1. NaBu inhibits the progression of endometrial cancer in vivo and in vitro

NaBu exerts a tumor suppressor role in a variety of tumors. Therefore, in this study, we used the CCK8 cell counting assay to detect the half-inhibitory concentration of NaBu in Ishikawa cells and HEC-1B cells after 24 hours of incubation. The results showed that the half-inhibitory concentration of NaBu in Ishikawa cells was 8.890 mM, and the half-inhibitory concentration in HEC-1B cells was 96.11 mM (Fig. 1A and B). Therefore, in the subsequent experiments, NaBu was used at a concentration of 5 mM for a duration of 24 hours. Next, endometrial cancer cells were treated with NaBu, and the effects of NaBu were explored using a CCK8 assay, clone formation assay, EdU cell proliferation assay kit, Transwell migration and invasion assay, and flow cytometry. The results showed that NaBu inhibited the viability of Ishikawa and HEC-1B cells in a time-dependent manner (Fig. 1C). NaBu inhibited the colony forming ability, proliferation ability, and migration and invasion abilities of Ishikawa and HEC-1B cells (Fig. 1D-F). NaBu promoted G2/M phase arrest in endometrial cancer cells, and the proportion of G1 phase and S phase cells was reduced accordingly (Fig. 1G). Finally, subcutaneous xenograft models were constructed to explore the effects of NaBu on endometrial cancer in vivo. Studies have shown that NaBu inhibits the progression of endometrial cancer in vivo (Fig. 1H). Mouse tumor volume and tumor weight were significantly reduced after NaBu treatment (Fig. 1I and J).

3.2. NaBu promotes endometrial cancer cell ferroptosis

NaBu inhibits the progression of endometrial cancer in vivo and in vitro. Next, metabolomic and transcriptomic analysis of HEC-1B cells treated with NaBu were performed to explore the underlying mechanism by which NaBu inhibits the progression of endometrial cancer. The levels of GSSG were elevated, and the levels of GSH and L-cysteine were significantly decreased after NaBu treatment (Fig. 2A). The results of KEGG enrichment analysis showed that glutathione metabolism was significantly changed after NaBu treatment (Fig. 2B). The expression level of SLC7A11 was significantly downregulated after NaBu treatment (Fig. 2C). SLC7A11 encodes a key component of the cystine-glutamate transporter, mediates glutathione biosynthesis and is closely related to ferroptosis. Therefore, we speculated that NaBu may promote ferroptosis in endometrial cancer cells by inhibiting glutathione biosynthesis through downregulation of the expression of SLC7A11. Next, we explored the relationship between NaBu and ferroptosis. qRT–PCR and Western blotting were used to detect the expression levels of SLC7A11 after NaBu treatment in Ishikawa cells and HEC-1B cells. The expression levels of SLC7A11 were decreased after NaBu treatment (Fig. 2D and E). The glutathione metabolism results showed that the ratio of GSH/GSSG decreased after NaBu treatment (Fig. 2F). Transmission electron microscopy was

used to observe the morphological changes of mitochondria in endometrial cancer cells after NaBu treatment. The results showed that the mitochondrial volume in endometrial cancer cells decreased and the number of mitochondrial cristae were significantly reduced after NaBu treatment (Fig. 2G).

Next, we explored the effects of NaBu on ROS, lipid ROS and intracellular Fe2 + in Ishikawa and HEC-1B cells. The results showed that NaBu increased the levels of ROS, lipid ROS and intracellular Fe2 + in Ishikawa and HEC-1B cells (Fig. 3A-C). Finally, DFO was used to observe whether the biological functions of NaBu could be reversed by DFO. The results showed that the effects of NaBu, which promoted cell viability and elevated the level of lipid ROS, were partially reversed by DFO (Fig. 3D and E).

3.3. NaBu promotes ferroptosis in endometrial cancer cells by inhibiting SLC7A11-dependent glutathione synthesis

The regulatory relationship between NaBu and SLC7A11 indicated that SLC7A11 may mediate the biological functions of NaBu. SLC7A11 was overexpressed in Ishikawa and HEC-1B cells to explore the role of SLC7A11 in NaBu-induced ferroptosis. The results showed that overexpression of SLC7A11 could partially reverse the biological functions of NaBu, which inhibited the cell viability and clone formation ability of Ishikawa and HEC-1B cells (Fig. 4A and B). Overexpression of SLC7A11 partially reversed the biological effects of NaBu, which reduced the GSH/GSSG ratio and increased the levels of ROS and lipid ROS in Ishikawa and HEC-1B cells (Fig. 4C-E).

3.4. RBM3 negatively regulates SLC7A11 expression

NaBu is an important histone deacetylase inhibitor that promotes transcription. In this study, NaBu inhibited the expression of SLC7A11. RNA-binding proteins are an important class of protein molecules involved in the post-transcriptional modification of RNA. Therefore, we speculated that NaBu may indirectly regulate the expression of SLC7A11 through RNA-binding proteins. To explore the mechanism, RNA pulldown experiments combined with mass spectrometry were used to screen the RNA-binding proteins that have a binding relationship with SLC7A11 mRNA. The results showed that RBM3 had a binding relationship with SLC7A11 mRNA (Fig. 5A and Supplementary table 1). Next, Western blotting was used to detect the expression levels of RBM3 and SLC7A11 in endometrial cancer cells after NaBu treatment. The results showed that the expression levels of RBM3 were increased and the expression levels of SLC7A11 were decreased in endometrial cancer cells after NaBu treatment (Fig. 5B).

3.5. RBM3 promotes ferroptosis in endometrial cancer cells

Next, RBM3 was overexpressed in Ishikawa and HEC-1B cells to explore the effects of RBM3 on ferroptosis. qRT–PCR and Western blotting were used to detect the regulatory relationship between RBM3 and SLC7A11. The results showed that the overexpression of RBM3 inhibited the expression of SLC7A11 in Ishikawa cells and HEC-1B cells (Fig. 5C and D). Experiments were conducted to explore the role of RBM3 in ferroptosis. The results of the CCK8 and clone formation assays showed that RBM3 overexpression inhibited the viability and clone formation ability of Ishikawa and HEC-1B cells (Fig. 5E and E). The results of the glutathione metabolism assay showed that overexpression of RBM3 decreased

the ratio of GSH/GSSG (Fig. 5G). Overexpression of RBM3 increased the levels of ROS and lipid ROS in Ishikawa and HEC-1B cells (Fig. 5H and I). Taken together, RBM3 promotes ferroptosis in endometrial cancer cells.

3.6. Sodium butyrate promotes ferroptosis in endometrial cancer cells by regulating the expression of RBM3

The regulatory relationship among NaBu, RBM3 and SLC7A11 indicated that RBM3 may mediate the biological functions of NaBu. RBM3 was downregulated in Ishikawa and HEC-1B cells. qRT–PCR and Western blotting were used to explore this regulatory relationship. The results showed that silencing RBM3 promoted the expression of SLC7A11 and partially reversed the biological effect of NaBu, which inhibited the expression of SLC7A11 (Fig. 6A and B). Next, experiments were conducted to explore the role of RBM3 in the process of NaBu-induced ferroptosis. The results of the CCK8 and clone formation assays showed that silencing RBM3 partially reversed the biological effects of NaBu, which inhibited the cell viability and clone formation ability of endometrial cancer cells (Fig. 6C and D). The results of the glutathione metabolism assay showed that silencing RBM3 partially reversed the biological effect of NaBu, which reduced the ratio of GSH/GSSG (Fig. 6E). The results of flow cytometry showed that silencing RBM3 partially reversed the biological effects of NaBu, which increased the levels of ROS and lipid ROS (Fig. 6F and G). Therefore, RBM3 mediated the biological functions of NaBu.

3.7. RBM3 promotes ferroptosis in endometrial cancer cells by downregulating SLC7A11 expression

The regulatory relationship between RBM3 and SLC7A11 indicated that RBM3 may promote ferroptosis by regulating the expression of SLC7A11. Next, experiments were conducted to explore whether SLC7A11 mediates the biological functions of RBM3. The results of the CCK8 and clone formation assays showed that overexpression of SLC7A11 partially reversed the biological effects of RBM3, which inhibited cell activity and clone formation ability (Fig. 7A and B). The results of flow cytometry showed that overexpression of SLC7A11 partially reversed the biological effects of RBM3, which increased the levels of ROS and lipid ROS (Fig. 7C and D). Subcutaneous graft tumor models were constructed to explore the biological effects of NaBu and RBM3 in vivo. The results showed that NaBu inhibited tumor growth in vivo and that silencing RBM3 promoted the growth of endometrial cancer in vivo (Fig. 7E). Mouse tumor weight and tumor volume were significantly reduced after NaBu treatment and RBM3 silencing (Fig. 7F and G).

4. Discussion

Recently, researchers have found that the gut microbiota plays an important role in the progression of various diseases[28, 29]. A previous study by our group found that the abundance of butyric acid-producing bacteria in the gut was significantly downregulated in a mouse model of endometrial dysplasia induced by a high-sugar and high-fat diet (unpublished manuscript). Butyric acid is one of the short-chain fatty acids produced by the gut microbiota through the fermentation of dietary fiber[30].

Butyric acid is closely related to the occurrence and development of various diseases. For example, short-chain fatty acids can inhibit LPC-induced demyelination, enhance remyelination and promote the differentiation of oligodendrocytes[31]. Butyric acid can enhance the functions of the intestinal barrier, activate the FFA2 receptor-mediated PI3K/Akt/mTOR pathway and exert a protective effect on muscle atrophy[32]. NaBu is closely related to the occurrence and development of tumors. For example, butyric acid promotes the immune response of CD8 + T cells in an ID2-dependent manner, thereby promoting the efficacy of antitumor therapy[33]. In liver cancer, butyric acid promotes the production of ROS via the miR-22/SIRT-1 axis, which in turn promotes apoptosis and inhibits the progression of liver cancer[10]. In endometrial cancer, NaBu can inhibit the progression of endometrial cancer; however, the specific mechanism is unclear[34]. In this study, we experimentally verified that butyric acid plays a key role in the progression of endometrial cancer.

Ferroptosis is a new form of programmed cell death mainly caused by the dysregulation of antioxidant/oxidative systems, iron metabolism and fatty acid metabolism[13]. SLC7A11 encodes a key component of the cystine/glutamate transporter, which promotes the intracellular transport of cystine, thereby promoting the biosynthesis of glutathione and enhancing the functions of the intracellular antioxidant system[35]. SLC7A11 exerts tumor-promoting effects in a variety of tumors. For example, in lung cancer, the stem cell factor SOX2 enhances stem cell resistance to ferroptosis by promoting the expression of SLC7A11[36]. In ovarian cancer, a PARP inhibitor was found to reduce the expression of SLC7A11 in a p53-dependent manner and then promote ferroptosis in tumor cells[37]. In endometrial cancer, the function of SLC7A11 has not been reported. In this study, through metabolomic and transcriptomic analysis, we found that glutathione metabolism and SLC7A11 expression were inhibited in endometrial cancer cells after NaBu treatment. NaBu can promote ferroptosis in endometrial cancer cells by inhibiting SLC7A11 expression.

RBM3 is an RNA-binding protein that is widely involved in multiple post-transcriptional modification events, such as RNA splicing, RNA transport, RNA sequence editing, RNA intracellular localization and translation, by binding and interacting with RNA[38–42]. RBM3 can play a dual role in tumors. For example, in breast cancer, RBM3 promotes the expression of ARPC2 by binding to the 3'UTR of ARPC2, thereby exerting a cancer-promoting effect[43]. In epithelial ovarian cancer, patients with high RBM3 expression have a better prognosis and are more sensitive to chemotherapy drugs[44]. In endometrial cancer, the function of RBM3 is unclear. In this study, we found that RBM3 binds to SLC7A11 mRNA and negatively regulates the expression of SLC7A11. NaBu indirectly regulates the expression of SLC7A11 by promoting the expression of RBM3, thereby promoting ferroptosis in endometrial cancer cells.

In conclusion, our study revealed the biological significance of NaBu, SLC7A11 and RBM3 in endometrial cancer. NaBu can promote ferroptosis in endometrial cancer cells through the RBM3/SLC7A11 axis. NaBu/RBM3/SLC7A11 signaling may be a novel target for the diagnosis and treatment of endometrial cancer.

Abbreviations

NaBu, Sodium Butyrate; ROS, reactive oxygen species; PBS, phosphate buffered solution; DFO, Deferoxamine mesylate; DMSO, Dimethyl sulfoxide; CCK8, Cell Counting Kit-8; Lipid ROS, lipid peroxidation; HRP, horseradish peroxidase; GSSG, oxidized glutathione; GSH, glutathione.

Declarations

Ethics approval and consent to participate

All animal studies were approved by the Institutional Animal Care and Use Committee Tongji Medical College, Huazhong University of Science and Technology (Permit No. S2717).

Consent for publication

If any individual or any person in this document needs the consent of another person to publish certain data, you must first obtain the consent of others before stating it here.

Competing interests

The authors declare that the research was conducted in the absence of any commercial or financial relationships that could be construed as a potential conflict of interest.

Funding

This study was financially supported by National Natural Science Foundation of China Grant (No. 81974409), the Fundamental Research Funds for the Central Universities (No. 2021yjsCXCY115), Major Technical Innovation Project in Hubei Province of China (2019ACA138) and the Fundamental Research Funds for the Central Universities (2019kfyXKJC072).

Authors' contributions

W.Z.W. designed and wrote the manuscript and performed most experiments. W.Z.W. and S.W. performed some experiments and edited the manuscript. W.Z.W., L.Y. and W.H.B contributed to the design of the study and reviewed and edited the manuscript. All authors read and approved the final manuscript.

Acknowledgements

We are very grateful for the guidance of our cooperative partner, Professor Toshimori Kitami.

Availability of data and material

The data used or analyzed during the current study are available from the corresponding author on reasonable request.

References

1. R.L. Siegel, K.D. Miller, H.E. Fuchs, et al., *Cancer statistics, 2022.* CA: A Cancer Journal for Clinicians, 2022. **72**(1): p. 7-33.
2. V. Makker, H. Mackay, I. Ray-Coquard, et al., *Endometrial cancer.* Nature Reviews Disease Primers, 2021. **7**(1): p. 88.
3. J.B. Pakish, K.H. Lu, C.C. Sun, et al., *Symptoms of endometrial cancer.* Journal of Clinical Oncology, 2015. **33**(15_suppl): p. e16501-e16501.
4. F. Amant, P. Moerman, P. Neven, et al., *Endometrial cancer.* The Lancet, 2005. **366**(9484): p. 491-505.
5. M.M. Braun, E.A. Overbeek-Wager, and R.J. Grumbo, *Diagnosis and Management of Endometrial Cancer.* Am Fam Physician, 2016. **93**(6): p. 468-74.
6. R.A. Brooks, G.F. Fleming, R.R. Lastra, et al., *Current recommendations and recent progress in endometrial cancer.* CA: A Cancer Journal for Clinicians, 2019. **69**(4): p. 258-279.
7. N. Sugimura, Q. Li, E.S.H. Chu, et al., *Lactobacillus gallinarum modulates the gut microbiota and produces anti-cancer metabolites to protect against colorectal tumourigenesis.* Gut, 2021: p. gutjnl-2020-323951.
8. M. Matsushita, K. Fujita, T. Hayashi, et al., *Gut Microbiota–Derived Short-Chain Fatty Acids Promote Prostate Cancer Growth via IGF1 Signaling.* Cancer Research, 2021. **81**(15): p. 4014-4026.
9. M.H. Vetter, B. Smith, J. Benedict, et al., *Preoperative predictors of endometrial cancer at time of hysterectomy for endometrial intraepithelial neoplasia or complex atypical hyperplasia.* American Journal of Obstetrics and Gynecology, 2020. **222**(1): p. 60.e1-60.e7.
10. K. Pant, A.K. Yadav, P. Gupta, et al., *Butyrate induces ROS-mediated apoptosis by modulating miR-22/SIRT-1 pathway in hepatic cancer cells.* Redox Biology, 2017. **12**: p. 340-349.
11. V. Salimi, M. Shabani, M. Nourbakhsh, et al., *Involvement of 15-lipoxygenase-1 in the regulation of breast cancer cell death induced by sodium butyrate.* Cytotechnology, 2016. **68**(6): p. 2519-2528.
12. Q. Li, C. Ding, T. Meng, et al., *Butyrate suppresses motility of colorectal cancer cells via deactivating Akt/ERK signaling in histone deacetylase dependent manner.* Journal of Pharmacological Sciences, 2017. **135**(4): p. 148-155.
13. X. Chen, J. Li, R. Kang, et al., *Ferroptosis: machinery and regulation.* Autophagy, 2021. **17**(9): p. 2054-2081.
14. P. Koppula, L. Zhuang, and B. Gan, *Cystine transporter SLC7A11/xCT in cancer: ferroptosis, nutrient dependency, and cancer therapy.* Protein & Cell, 2021. **12**(8): p. 599-620.
15. X. Bai, J. Ni, J. Beretov, et al., *Activation of the eIF2α/ATF4 axis drives triple-negative breast cancer radioresistance by promoting glutathione biosynthesis.* Redox Biology, 2021. **43**: p. 101993.
16. L. Ma, T. Chen, X. Zhang, et al., *The m6A reader YTHDC2 inhibits lung adenocarcinoma tumorigenesis by suppressing SLC7A11-dependent antioxidant function.* Redox Biology, 2021. **38**: p. 101801.
17. S. Wang, W. Li, P. Zhang, et al., *Mechanical overloading induces GPX4-regulated chondrocyte ferroptosis in osteoarthritis via Piezo1 channel facilitated calcium influx.* Journal of Advanced

Research, 2022.

18. Y. Lu, Y.-T. Chan, H.-Y. Tan, et al., *Epigenetic regulation of ferroptosis via ETS1/miR-23a-3p/ACSL4 axis mediates sorafenib resistance in human hepatocellular carcinoma.* Journal of Experimental & Clinical Cancer Research, 2022. **41**(1): p. 3.
19. Y.Y. Zhang, Z.J. Ni, E. Elam, et al., *Juglone, a novel activator of ferroptosis, induces cell death in endometrial carcinoma Ishikawa cells.* Food Funct, 2021. **12**(11): p. 4947-4959.
20. Y. Fukuda, M.F. Pazyra-Murphy, E.S. Silagi, et al., *Binding and transport of SFPQ-RNA granules by KIF5A/KLC1 motors promotes axon survival.* Journal of Cell Biology, 2020. **220**(1).
21. D. Li, J. Liu, C. Yang, et al., *Targeting long noncoding RNA PMIF facilitates osteoprogenitor cells migrating to bone formation surface to promote bone formation during aging.* Theranostics, 2021. **11**(11): p. 5585-5604.
22. F. Xiong, R. Wang, J.-H. Lee, et al., *RNA m6A modification orchestrates a LINE-1–host interaction that facilitates retrotransposition and contributes to long gene vulnerability.* Cell Research, 2021. **31**(8): p. 861-885.
23. Q. Guo, Y. Wu, X. Guo, et al., *The RNA-Binding Protein CELF2 Inhibits Ovarian Cancer Progression by Stabilizing FAM198B.* Molecular Therapy - Nucleic Acids, 2021. **23**: p. 169-184.
24. X. Miao and N. Zhang, *Role of RBM3 in the regulation of cell proliferation in hepatocellular carcinoma.* Experimental and Molecular Pathology, 2020. **117**: p. 104546.
25. T. Sakurai, H. Kashida, Y. Komeda, et al., *Stress Response Protein RBM3 Promotes the Development of Colitis-associated Cancer.* Inflammatory Bowel Diseases, 2017. **23**(1): p. 57-65.
26. N. Melling, K. Bachmann, B. Hofmann, et al., *Prevalence and clinical significance of RBM3 immunostaining in non-small cell lung cancers.* Journal of Cancer Research and Clinical Oncology, 2019. **145**(4): p. 873-879.
27. H.-J. Yang, F. Ju, X.-X. Guo, et al., *RNA-binding protein RBM3 prevents NO-induced apoptosis in human neuroblastoma cells by modulating p38 signaling and miR-143.* Scientific Reports, 2017. **7**(1): p. 41738.
28. Z.-X. Chen, J.-L. Li, P. Pan, et al., *Combination gut microbiota modulation and chemotherapy for orthotopic colorectal cancer therapy.* Nano Today, 2021. **41**: p. 101329.
29. J. Hong, F. Guo, S.-Y. Lu, et al., *F. nucleatum targets lncRNA ENO1-IT1 to promote glycolysis and oncogenesis in colorectal cancer.* Gut, 2021. **70**(11): p. 2123-2137.
30. H. Liu, J. Wang, T. He, et al., *Butyrate: A Double-Edged Sword for Health?* Advances in Nutrition, 2018. **9**(1): p. 21-29.
31. T. Chen, D. Noto, Y. Hoshino, et al., *Butyrate suppresses demyelination and enhances remyelination.* Journal of Neuroinflammation, 2019. **16**(1): p. 165.
32. G. Tang, Y. Du, H. Guan, et al., *Butyrate ameliorates skeletal muscle atrophy in diabetic nephropathy by enhancing gut barrier function and FFA2-mediated PI3K/Akt/mTOR signals.* British Journal of Pharmacology, 2022. **179**(1): p. 159-178.

33. Y. He, L. Fu, Y. Li, et al., *Gut microbial metabolites facilitate anticancer therapy efficacy by modulating cytotoxic CD8+ T cell immunity.* Cell Metabolism, 2021. **33**(5): p. 988-1000.e7.
34. N. Takai, J.C. Desmond, T. Kumagai, et al., *Histone Deacetylase Inhibitors Have a Profound Antigrowth Activity in Endometrial Cancer Cells.* Clinical Cancer Research, 2004. **10**(3): p. 1141.
35. M.P. Murphy, *Metabolic control of ferroptosis in cancer.* Nature Cell Biology, 2018. **20**(10): p. 1104-1105.
36. X. Wang, Y. Chen, X. Wang, et al., *Stem Cell Factor SOX2 Confers Ferroptosis Resistance in Lung Cancer via Upregulation of SLC7A11.* Cancer Research, 2021. **81**(20): p. 5217.
37. T. Hong, G. Lei, X. Chen, et al., *PARP inhibition promotes ferroptosis via repressing SLC7A11 and synergizes with ferroptosis inducers in BRCA-proficient ovarian cancer.* Redox Biology, 2021. **42**: p. 101928.
38. X. Wang, C. Ping, P. Tan, et al., *hnRNPLL controls pluripotency exit of embryonic stem cells by modulating alternative splicing of Tbx3 and Bptf.* The EMBO Journal, 2021. **40**(4): p. e104729.
39. L. Olgeiser, C. Haag, S. Boerner, et al., *The key protein of endosomal mRNP transport Rrm4 binds translational landmark sites of cargo mRNAs.* EMBO reports, 2019. **20**(1): p. e46588.
40. G. Quinones-Valdez, S.S. Tran, H.-I. Jun, et al., *Regulation of RNA editing by RNA-binding proteins in human cells.* Communications Biology, 2019. **2**(1): p. 19.
41. R. Satoh, K. Hagihara, and R. Sugiura, *Rae1-mediated nuclear export of Rnc1 is an important determinant in controlling MAPK signaling.* Current Genetics, 2018. **64**(1): p. 103-108.
42. A. Sasse, K.U. Laverty, T.R. Hughes, et al., *Motif models for RNA-binding proteins.* Current Opinion in Structural Biology, 2018. **53**: p. 115-123.
43. P. Chen, X. Yue, H. Xiong, et al., *RBM3 upregulates ARPC2 by binding the 3'UTR and contributes to breast cancer progression.* Int J Oncol, 2019. **54**(4): p. 1387-1397.
44. Å. Ehlén, D.J. Brennan, B. Nodin, et al., *Expression of the RNA-binding protein RBM3 is associated with a favourable prognosis and cisplatin sensitivity in epithelial ovarian cancer.* Journal of Translational Medicine, 2010. **8**(1): p. 78.

Figures

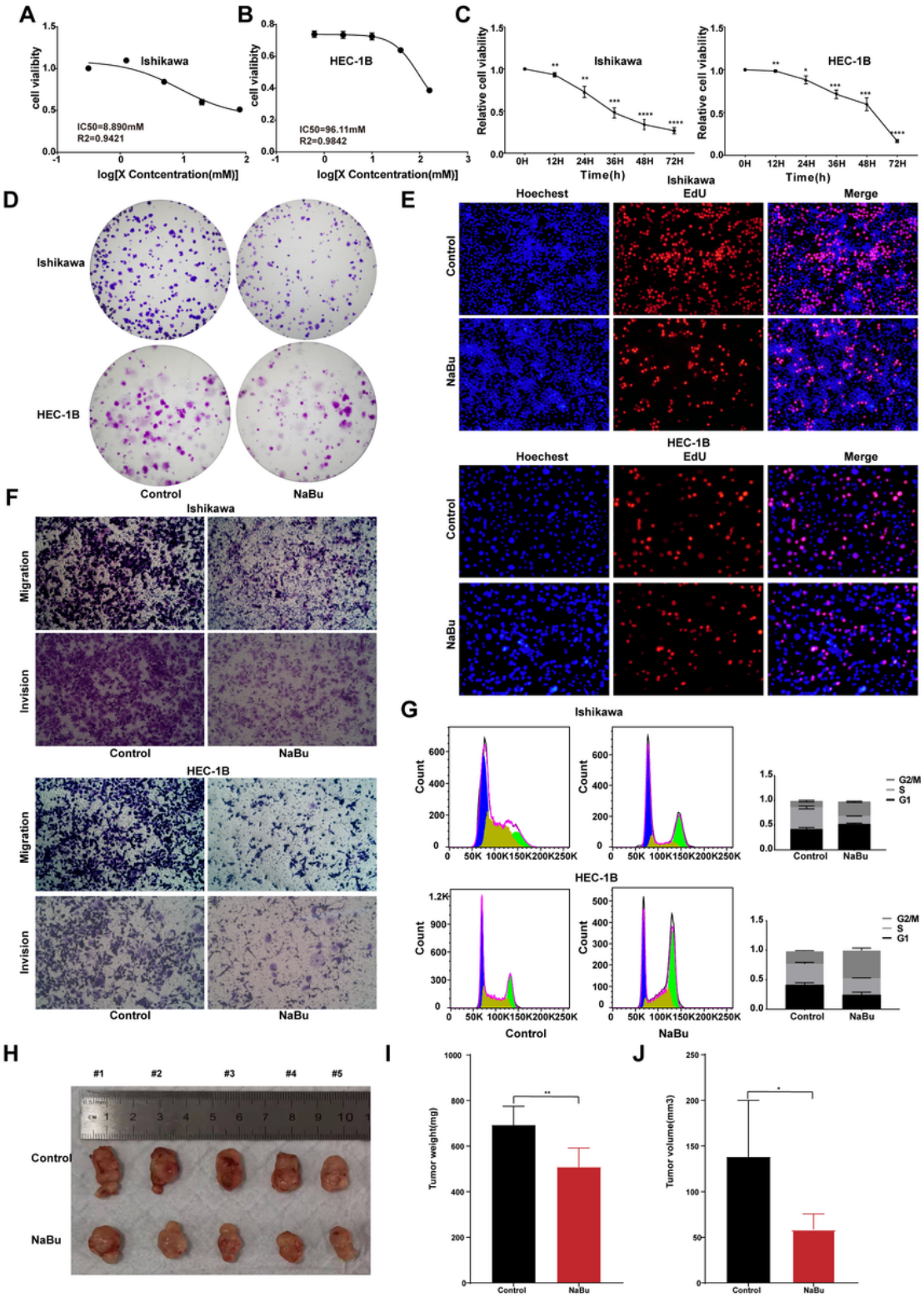

Figure 1

NaBu inhibits the progression of endometrial cancer in vivo and in vitro.(A-B) IC50 curves constructed with the CCK8 results after NaBu treatment for 24 hours. (C) Cell viabilities were assayed by CCK8 assay after treatment with 5 mM NaBu for 0 hours, 12 hours, 24 hours, 36 hours, 48 hours and 72 hours. (D) Colony formation of Ishikawa and HEC-1B cells measured with a colony formation assay after NaBu treatment. (E) EdU proliferation assay kits were used to detect the proliferation ability of Ishikawa and

HEC-1B cells after NaBu treatment. (F) The migration and invasion abilities of Ishikawa and HEC-1B cells were assayed in Transwell chambers after NaBu treatment. (G) The cell cycle distribution of Ishikawa and HEC-1B cells was measured by flow cytometry after NaBu treatment. (H) Tumor image of the subcutaneous xenograft model at 28 days. (I) Tumor weights of each group in the subcutaneous xenograft model at 28 days. (J) Tumor volumes in each group of mice in the subcutaneous xenograft model at 28 days. ns P>0.05, *P<0.05, **P<0.01, ***P<0.001, ****P<0.0001.

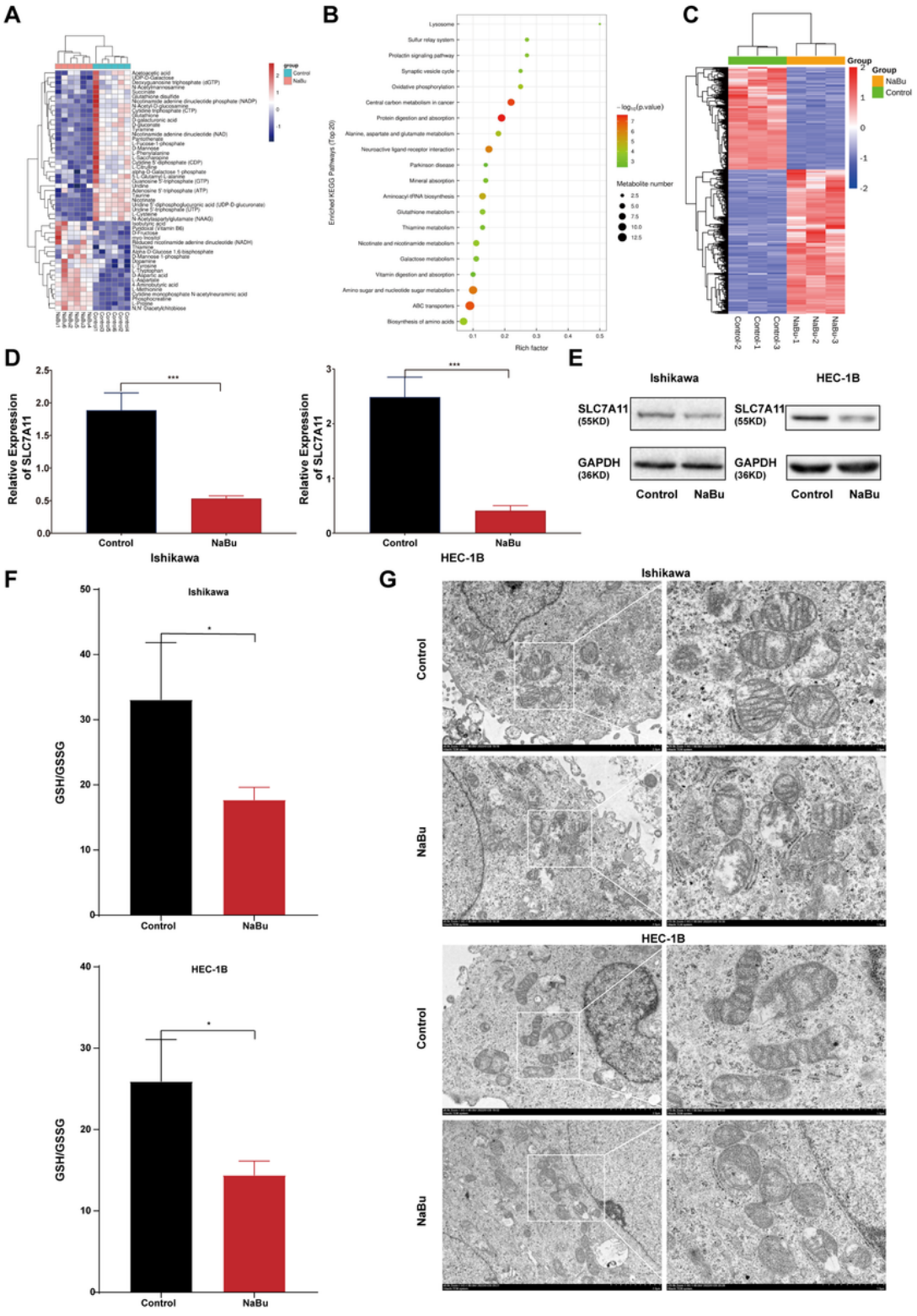

Figure 2

NaBu promotes ferroptosis of endometrial cancer cells. (A) Cluster heatmap of differential metabolites. (B) KEGG enrichment analysis of differential metabolites. (C) Cluster heatmap of differentially expressed genes. (D-E) qRT–PCR and Western blotting were used to detect the expression levels of SLC7A11 at the mRNA and protein levels after NaBu treatment in Ishikawa and HEC-1B cells. (F) Glutathione metabolism was assayed by GSH and GSSG assay kits after NaBu treatment in Ishikawa and HEC-1B cells. (G) Transmission electron microscopy was used to observe the morphological changes of Ishikawa and HEC-1B cells after NaBu treatment. ns P>0.05, *P<0.05, **P<0.01, ***P<0.001, ****P<0.0001.

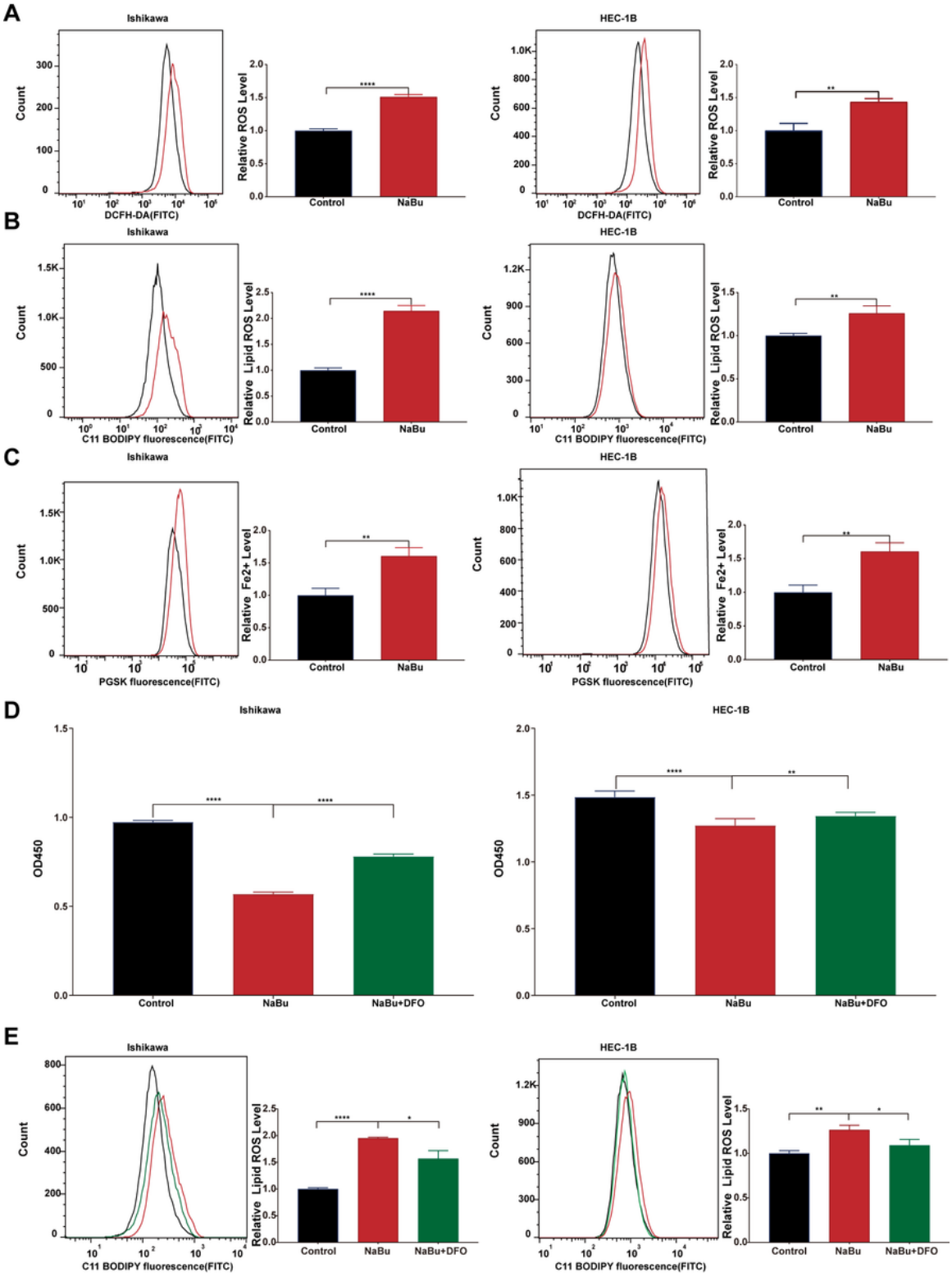

Figure 3

NaBu promotes ferroptosis in endometrial cancer cells. (A) DCFH-DA probes were used to detect the level of ROS in Ishikawa and HEC-1B cells after NaBu treatment. (B) C11-BODIPY probes were used to detect the level of lipid ROS in Ishikawa and HEC-1B cells after NaBu treatment. (C) Phen Green™ SK probes were used to detect the level of Fe2+ in Ishikawa and HEC-1B cells after NaBu treatment. (D) The viability of Ishikawa and HEC-1B cells was assayed by CCK8 after NaBu treatment in the presence or absence of

DFO. (E) The level of lipid ROS was assayed with C11-BODIPY probes after NaBu treatment in the presence or absence of DFO. ns P>0.05, *P<0.05, **P<0.01, ***P<0.001, ****P<0.0001.

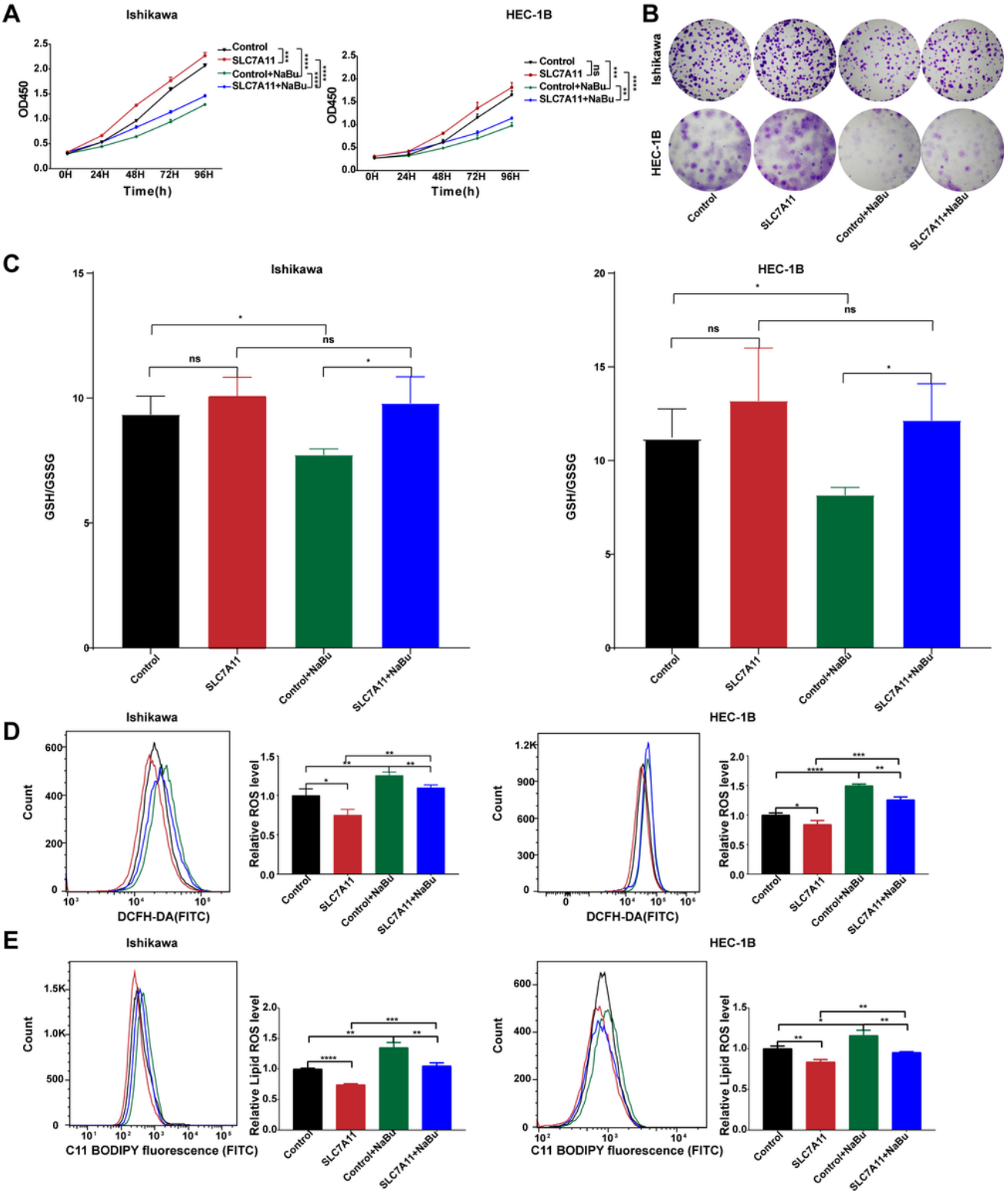

Figure 4

NaBu promotes ferroptosis in endometrial cancer cells by inhibiting SLC7A11-dependent glutathione synthesis. (A-B) SLC7A11 was overexpressed in Ishikawa and HEC-1B cells, and the cell viability and

clone formation ability were measured by CCK8 and clone formation assays in the presence or absence of NaBu. (C) SLC7A11 was overexpressed in Ishikawa and HEC-1B cells, and glutathione metabolism was assayed with GSH and GSSG assay kits in the presence or absence of NaBu. (D-E) SLC7A11 was overexpressed in Ishikawa and HEC-1B cells, and the levels of ROS and lipid ROS were assayed by flow cytometry in the presence or absence of NaBu. ns P>0.05, *P<0.05, **P<0.01, ***P<0.001, ****P<0.0001.

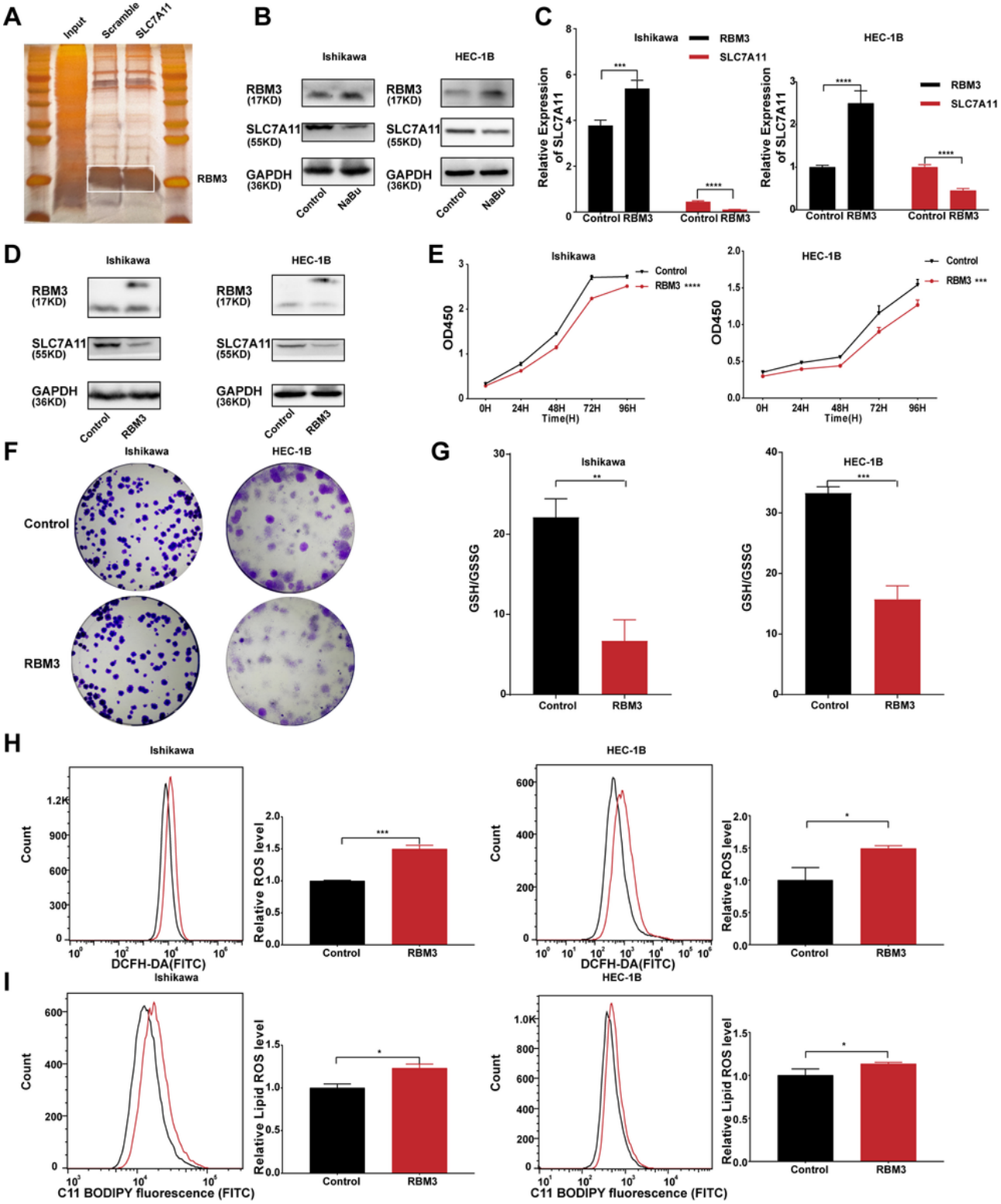

Figure 5

RBM3 negatively regulates SLC7A11 expression. (A) The results of silver staining showed that RBM3 had a mutual binding relationship with SLC7A11 mRNA. (B) Western blotting was used to detect the expression levels of RBM3 and SLC7A11 in Ishikawa and HEC-1B cells after treatment with NaBu. (C-D) RBM3 was overexpressed in Ishikawa and HEC-1B cells, and qRT–PCR and Western blotting were used to detect the expression levels of RBM3 and SLC7A11. (E-F) CCK8 and clone formation assays were used to detect the cell viability and clone formation ability of Ishikawa and HEC-1B cells after overexpression of RBM3. (G) GSH and GSSG assay kits were used to assay glutathione metabolism in Ishikawa and HEC-1B cells after RBM3 overexpression. (H-I) The levels of ROS and lipid ROS in Ishikawa and HEC-1B cells were assayed by flow cytometry after RBM3 overexpression. ns $P>0.05$, *$P<0.05$, **$P<0.01$, ***$P<0.001$, ****$P<0.0001$.

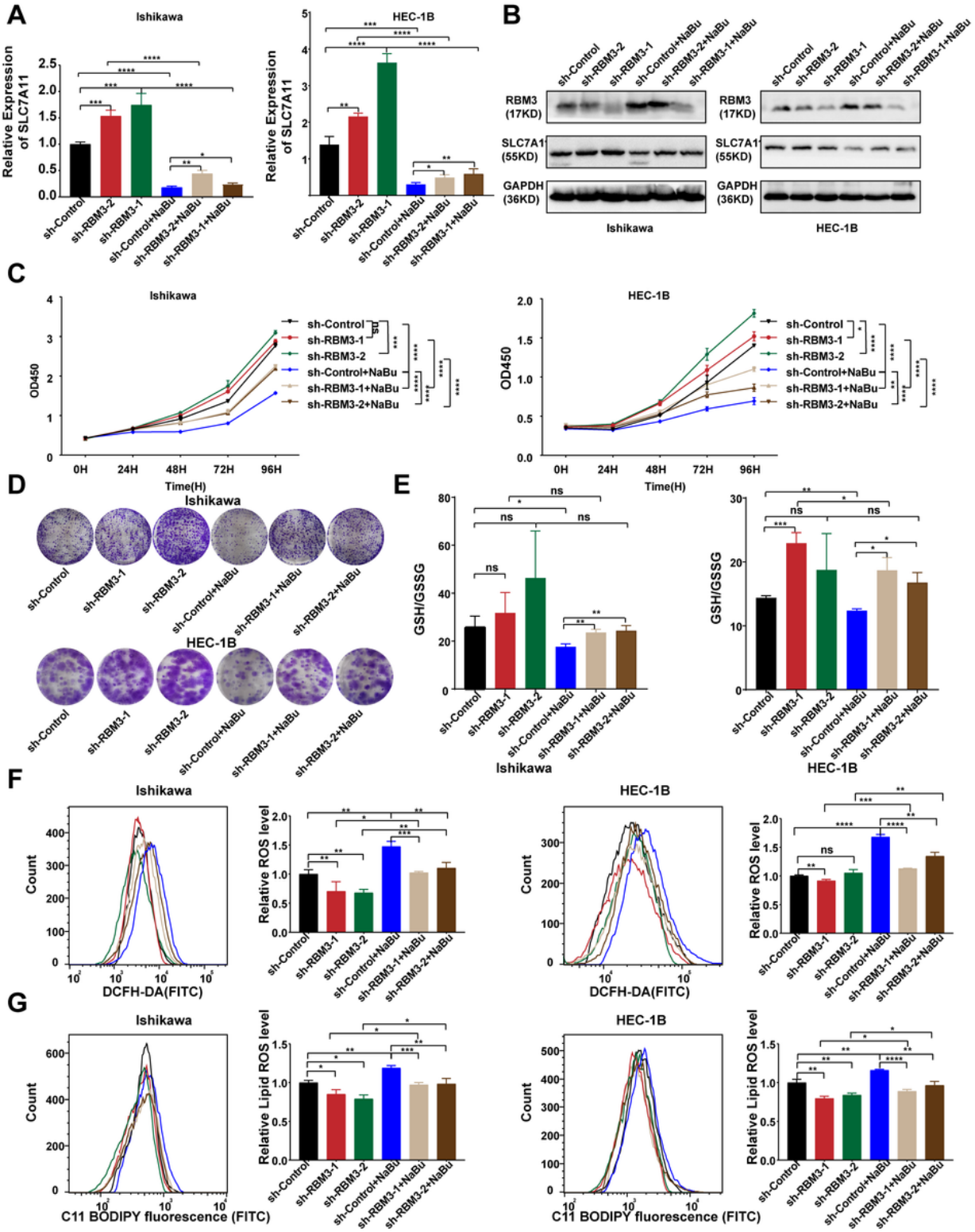

Figure 6

Sodium butyrate promotes ferroptosis in endometrial cancer cells by regulating the expression of RBM3. (A-B) RBM3 was downregulated in Ishikawa and HEC-1B cells, and the expression levels of SLC7A11 in Ishikawa and HEC-1B cells were assayed by qRT–PCR and Western blot in the presence or absence of NaBu. (C-D) RBM3 was downregulated in Ishikawa and HEC-1B cells, and CCK8 and clone formation assays were used to detect the cell viability and clone formation ability in the presence or absence of

NaBu. (E) RBM3 was downregulated in Ishikawa and HEC-1B cells, and glutathione metabolism was assayed using GSH and GSSG assay kits in the presence or absence of NaBu. (F-G) RBM3 was downregulated in Ishikawa and HEC-1B cells, and flow cytometry was used to detect the levels of ROS and lipid ROS in the presence or absence of NaBu. ns P>0.05, *P<0.05, **P<0.01, ***P<0.001, ****P<0.0001.

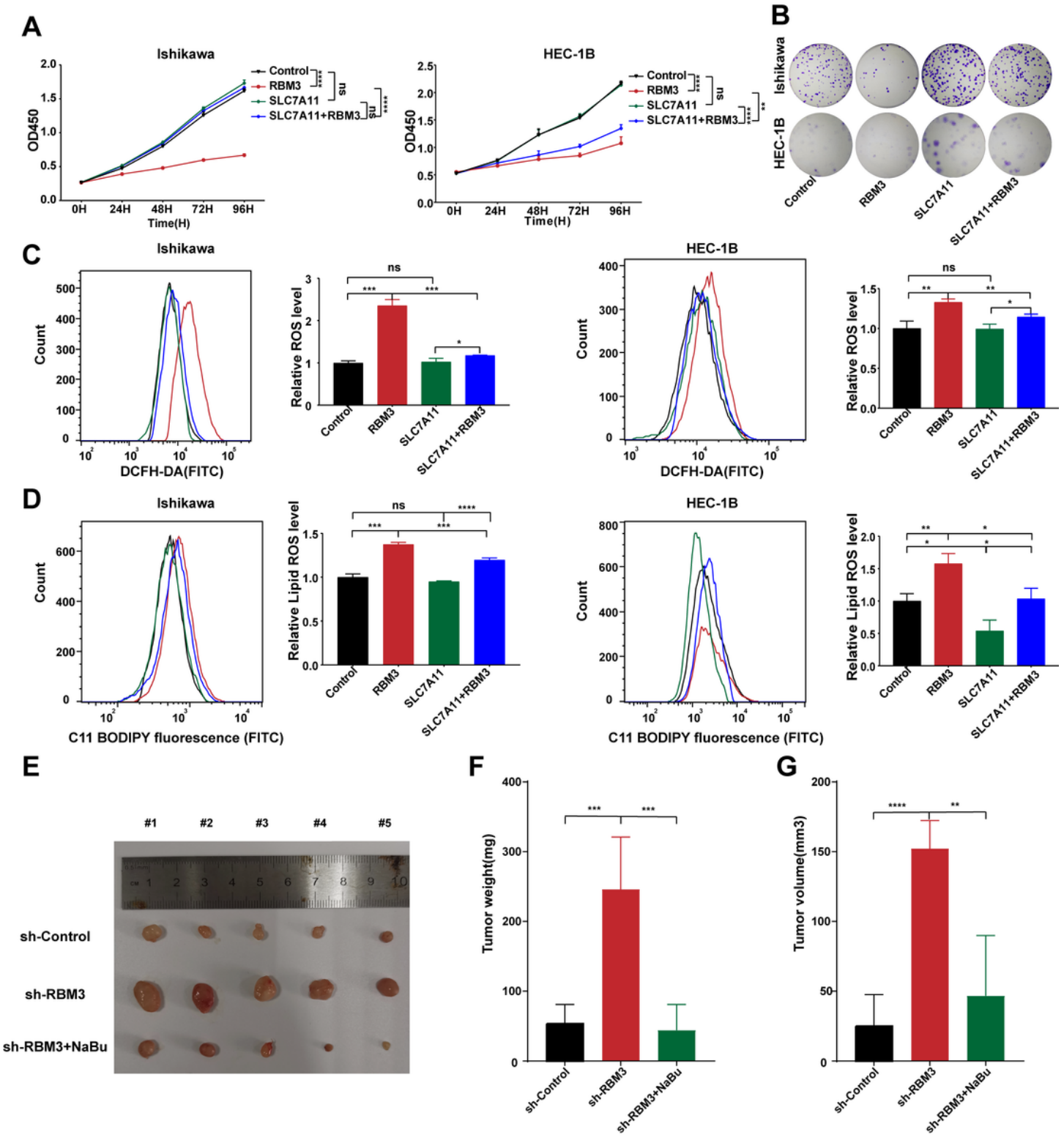

Figure 7

RBM3 promotes ferroptosis in endometrial cancer cells by downregulating SLC7A11 expression. (A-B) RBM3 and SLC7A11 overexpression vectors were co-transfected, and CCK8 and clone formation assays were used to compare the cell viability and clone formation ability in Ishikawa and HEC-1B cells. (C-D) RBM3 and SLC7A11 overexpression vectors were co-transfected, and the levels of ROS and lipid ROS were assayed by flow cytometry in Ishikawa and HEC-1B cells. (E) Tumor images of each group of mice in the subcutaneous xenograft model at 28 days. (F) Tumor weights of each group of mice in the subcutaneous xenograft model at 28 days. (G) Tumor volumes of each group of mice in the subcutaneous xenograft model at 28 days. ns P>0.05, *P<0.05, **P<0.01, ***P<0.001, ****P<0.0001.

Supplementary Files

This is a list of supplementary files associated with this preprint. Click to download.

- GA.png
- Supplementarytable1.xlsx